DEUTSCHES ELEKTRONEN-SYNCHROTRON DESY

DESY SR-79/28
October 1979

ION PAIR FORMATION FROM PHOTON IRRADIATION OF O_2, NO, AND CO FROM 17 TO 30 eV

by

H. Oertel, H. Schenk, H. Baumgärtel
Institut für Physikalische Chemie und Quantenchemie
der Freien Universität Berlin

NOTKESTRASSE 85 · 2 HAMBURG 52

To be sure that your preprints are promptly included in the
HIGH ENERGY PHYSICS INDEX ,
send them to the following address (if possible by air mail) :

DESY
Bibliothek
Notkestrasse 85
2 Hamburg 52
Germany

DESY SR-79/28
October 1979

ION PAIR FORMATION FROM PHOTON IRRADIATION OF O_2, NO, AND CO FROM 17 TO 30 eV

H. Oertel, H. Schenk, H. Baumgärtel
Institut für Physikalische Chemie und Quantenchemie
der Freien Universität Berlin
Takustraße 3, D-1000 Berlin 33

Abstract

Relative photoionization efficiency curves of the fragment ions of O_2, NO, and CO were determined in the energy region 17eV to 30eV by means of synchrotron radiation. The photoionization efficiency curves for O^- and O^+ from molecular oxygen, for O^- and N^+ from nitric oxide, and for O^- and C^+ and C^- from carbon monoxide were determined with a wavelength resolution of 0.2 nm. The data show predissociation structure in the ion pair formation region and autoionization structure in the region of dissociative ionization. Because the mass spectrometric determination of negative photoions exhibits a very low noise level, the investigation of ion pair formation processes provides considerable information on weak Rydberg series in the VUV energy region.

Introduction

For many years the atmospheric gases have been the subject of absorption- and photoionization-studies. Much work has been done in this field up to the photon energy 21eV.

A review article covering the work done for O_2 to about 1975 up to this energy is given by Dehmer and Chupka (1).

Recently the feasability of synchrotron radiation sources of high intensity gave rise to absorption measurements of O_2, NO, and CO in the energy region 21eV to 30eV.

For O_2, Codling and Madden (2) reported the relative absorption cross section in the 20.7eV to 24.8eV region, and Watson etal (3) published the absorption coefficients up to 31eV.

Absorption measurements for NO have been published from Narayana and Price (4) in the energy region 17eV to 24.8eV, and from Sasanuma etal (5). Hertz etal (6) determined the photoionization efficiency curves of NO^+, N^+, and O^+ in the region 18.5eV to 23eV.

The absorption spectrum of CO in the 19.6eV to 23.4eV energy region has been reported by Codling and Potts (7). Absorption cross sections in the energy region 17eV to 23.8eV have been published by Lee etal (8) and Sasanuma etal (9). Branching ratios up to 40eV for the dissociative ionization of O_2, NO, and CO have been measured by Kronebusch and Berkowitz (10), using line sources.

The present work deals with the ion pair formation processes. The mass spectrometric determination of the relative photoionization efficiency curves of O^-/O^+ from O_2, O^-/N^+ from NO and O^-/C^+ and C^- from CO is reported. The apparatus used in this study combines very low noise level for the negative ion detection and high photon intensity. This enables the study of the low intensity fragmentation processes

Experimental

The apparatus has been described in a previous paper (11). Briefly, the synchrotron radiation of the storage ring DORIS at DESY, Hamburg, was used as a light source. The radiation was dispersed by a normal incidence monochromator (12). The wavelength resolution amounts to 0.2 nm for all the measurements. The fragment ions were selected by a quadrupole mass filter and detected by a channel electron multiplier. Gases were used without further purification. The pressure in the ion source was held at about 4×10^{-5} Torr (5×10^{-3} Pa) during the measurements, to avoid secondary collision effects.

O_2

Previous mass spectrometric investigations of the photodissociation and photoionization of molecular oxygen have been performed by some groups using a helium continuum as the source of exciting radiation (1, 13, 14). The most recent measurements have been done by Dehmer and Chupka (1) with a wavelength resolution of 0.007 nm. They reported the relative photoionization efficiency curves for O_2^+ up to 21.3eV and the curves for O^- and O^+ up to 20.5eV.

Results

In fig 1 the O^--yield curve in the energy region 17eV to 27eV and the O^+-yield curve from 17eV to 29eV are shown.

The O^--curve exhibits two distinct regions. The initial steep onset of the first one lies at 17.28eV. Up to 18.4eV the O^--yield curve shows a large number of features. They have been investigated and interpreted extensively by Dehmer and Chupka (1). Although they reported that there was no discernable structure in the energy region 18.4eV to 20.6eV, we observed weak but reproducible structure.

The second region is shown in fig 2. The steep onset lies at 20.59eV, followed by some structure up to a second steep onset at 21.28eV. The intensity decreases above 21.5eV. On the declining slope some features were observed. The ratio of the O^--intensity at the first part maximum at 17.3eV to the second part maximum at 21.56eV is 2. The ratio of the O^-- to the O^+-intensity at 21.5eV is 0.024. These ratios are purely experimental and do not take into account discrimination effects of the mass filter.

Table 1 contains the O^--yield structure above 20.4eV together with data from electron-impact- and absorption-measurements. The absorption bands were classified by Codling and Madden (2) as Rydberg states converging to the v'=0 and v'=1 vibrational levels of the O_2^+-ion state $c^4\Sigma_u^-$. The assignment of the states is taken from Lindholm (15) and Narayana and Price (4).

Discussion

O^-

In the 17eV to 18.4eV energy region, the agreement with the photoionization efficiency curves of Dehmer and Chupka (1) is good. Between 18.4eV and 20.5eV we observed some structure in contrast to previous measurements. Candidates for neutral states predissociating in ion pair states could be the Rydberg states converging to the $B^2\Sigma_g^-$-ion state. The same neutral states are responsible for structure in the O^+-efficiency curve. The branching ratio of O^+- and O^--production from neutral states is about 100:1. The weakness of that structure prevents further interpretation. Continuum contributions seems to be absent.

At 20.59eV O^- and O^- may be formed in the ground state $^2P^o$ and in the first excited state $^2D^o$, respectively. A steep onset is observed at this energy. Combination of a $^2D^o$-term with a $^2P^o$-term gives rise to Σ^+, Σ^- (2), Σ(3), Δ (2), 4 molecular states with both singlet and triplet multiplicities. From these states $^3\Sigma_u^-$(2)- and $^3\Pi_u$(3)-states can be populated through a dipole allowed transition from the $^3\Sigma_g^-$-ground state. The width of the steep onset at 20.59eV amounts to the same value as the fwhm of the exciting radiation. For these reasons we describe the steep onset as due to direct dissociation via an ion pair state or via a Rydberg state with proper symmetry interacting sufficiently strongly with the corresponding ion state. This interaction would result in an avoided crossing which would lead to a potential curve with a double minimum with the intervening maximum below the asymptote (1). The same interpretation may hold for the onset at 21.28eV.

At 22.28eV, O^- and O^+ may be formed in the ground state and in the second excited state $^2P^o$, respectively. Optically allowed transitions from the O_2 ground state to the corresponding molecular states are possible. The onset at 22.46eV is interpreted as direct dissociation into $O^-(^2P^o)$+

$O^+(^2P^o)$. These interpretations of the onsets to direct fragmentation processes are supported by investigations of Locht etal (16). The onsets, observed by Locht etal (16) above 23.5eV by means of electron impact excitation, and interpreted as direct dissociation, have not been confirmed in the photoionisation efficiency curves. The processes should be optically forbidden, therefore.

Peak structures has been observed in the O^--efficiency curve in addition to the steep onsets. The peaks result from predissociating Rydberg states, converging to the $c^4\Sigma_u^-$-ion state. From all the Rydberg states, the $4sc_g(1,0)$-state gives the most intense contribution to the O^--yield (tab 1).

The same states give rise to peak structure in the O^+- and the O_2^+-photoionization efficiency curves and in the efficiency curve for the production of fluorescence in the wavelength region 105 nm - 180 nm, and 124 nm - 180 nm (17).

Rydberg states at 20.85eV and 21.05eV interact with the $O^-(^2P^o)$ + $O^+(^4S^o)$- and the $O^-(^2P^o)$ + $O^+(^2D^o)$-continuum, Rydberg states above 22.28eV interact with the $O^-(^2P^o)$ + $O^+(^2P^o)$-continuum additionally. Because of the interaction with different continua, one would expect different resonance profiles. This is observed in fact.

In absorption and in the O_2^+-efficiency curve, the members of both the nsc_g- and ndc_g-series been observed with asymmetric profiles. In fluorescence and in the O^+-efficiency curve, the Rydberg states have been observed with symmetric profiles. The resonances observed in the O^--efficiency curve seems to be slightly asymmetric.

Between 21.5eV and 22.4eV, further structure has been observed in the O^--efficiency curve. There are several pairs of peaks separated by about 180 meV. This is the energy difference of the v'=0 and v'=1 vibrational level

of the ion state $c^4\Sigma_u^-$. We interpret these structures as members of two Rydberg series with quantum defects of δ = 0.83 and δ = 0.65 (table 2). The peaks at 22.11eV and 22.27eV are also observed in fluorescence (17).

O^+

The O^+-photoionization efficiency curve agrees well with that of Dehmer and Chupka (1) up to 20.3eV. The lower wavelength resolution makes the continuum more intense relative to autoionization structure. In the 20.4eV to 30eV region, the O^+-yield exhibits an intense continuum contribution with a maximum at 23eV. The onset at 20.87eV has been interpreted as direct dissociation to O^+ and a neutral oxygen atom in the $^4S^o$-ground state and first excited ^1D-state, respectively. Rydberg states, discussed above, are responsible for structure above 22.5eV.

NO

Results

Figs 3 and 4 shows the results for nitric oxide: the relative photoionization efficiency curve for O^- in the energy region from 19eV to 25eV and the corresponding efficiency curve for N^+ are shown in fig 3. The N^+-efficiency curve in the whole energy region is shown in fig 4 separately. In table 3 the features observed in the ion pair formation yield are given with previous results from absorption measurements and electron-impact studies.

The O^--yield curve exhibits a steep onset at 19.56eV, followed by two strong peaks and some weak peaks and shoulders up to 21.5eV. After a steep ascent at 21.49eV, three broad bands emerge at 21.9eV, 23.1eV, and 24.5eV.

The N^+-yield curve resembles the same features as observed in the O^--yield up to about 21eV. The N^+-efficiency curve

slowly increases from 21eV in two steps (fig 3). At 21.74eV the N^+-curve shows a very steep ascent and again at about 22.9eV (fig 4).

Most of the features can be compared with known data. The values, summarized in column 3 and 4 of table 3, are taken from electron-impact work. Hierl etal (18) have measured the N^+-efficiency curve after excitation with 18eV to 25eV electrons. They found a contribution below the threshold energy for the dissociative ionization of NO and interpret it as due to ion pair formation. Locht etal (16) excited NO with 18eV to 30eV electrons and observed the O^--yield. From their data they obtained the onsets of several processes contributing to ion pair formation, which are mainly interpreted as direct dissociation processes. Column 5 of table 3 summarizes the known absorption bands (4). The bands are classified as Rydberg states converging to the limit 21.72eV.

From table 3 one can see the extent of the agreement between the onsets observed in electron impact studies, the absorption bands, and the features obtained in this work.

In addition to the known features, there is some new structure, which has been observed for the first time. An assignment of these structure is given.

Table 4 summarizes the calculated threshold energies for the formation of different ion pairs.

In table 5, the features in the dissociative ionization region (above 21.02eV) are collected. Threshold energies of the appearence of different fragments are given, too. There is no hint to the ion pair process $NO + h\nu \rightarrow N^- + O^+$ found in the mass spectrum.

Discussion

The N^+-efficiency curve resembles the features of the O^--yield curve below 21.0eV (fig 3). The N^+-yield curve is overlapped by contributions due to the efficiency of second order radiation of the monochromator grating. That is the reason why the N^+- and the O^--curve are not identical below 21.0eV. Above 21.0eV, dissociative ionization processes contribute to the N^+-yield curve. The NO^+ decays to positive ions and neutral oxygen atoms. The cross section for these processes is orders of magnitude larger than that for the ion pair processes. In this energy region, the ion pair formation cross section can be observed only in the O^--efficiency curve.

O^-

At the energy 19.56eV, O^- and N^+ may be formed in the $^2P^o$-ground state and in the $^3\Gamma$-ground state, respectively. This onset is observed in the efficiency curve. The ions are formed without kinetic energy at the onset. Since specific neutral molecular states are unknown in this region, our interpretation follows the discussion of Dehmer and Chupka (1). They have interpreted the ion pair formation in O_2 at the minimum energy of the process $O_2 + h\nu \rightarrow O^-(^2P^o) + O^+(^4S^o)$ at 17.27eV due to direct dissociation: they found the rotational states of the O_2-ground state as steps in the onset slope of the O^+-yield curve. Although the resolution of our monochromator does not enable a rotational analysis of the slope near threshold, we assume that the direct dissociation process as describing the decay of NO at 19.56eV. The shape of the curve in the onset region confirms the interpretation. The step ascent does not result from a resonant excitation process. The fragment's atomic states give rise to molecular states Σ, Π, and Δ with both doublet and quartet multiplicities. The dipole transition from the $^2\Pi$ NO ground state is allowed to the doublet states, leading to the ion pair formation.

The same interpretation holds for the next steep at 21.46eV. It is as distinct as the first one. The excitation energy enables the ion pair O^- and N^+ to be formed in the ground state, $^2P^o$, and in the first excited state, ^1D, respectively. The steepness of the slope and the threshold energy supports the interpretation as direct dissociation via the ion pair state. The combination of $^2P^o$ and ^1D terms gives rise to Σ, Π, Δ, and Φ states with doublet multiplicity. The three states Σ, Π, and Δ are allowed to be reached by photoexcitation from the NO ground state. Although neutral states are known to exist near 21.5eV - viz. Rydberg states converging to the ion state at 21.72eV - the contribution via predissociating Rydberg states should be small, because of the low transition probability into Rydberg states with large principle quantum numbers.

Between 20eV and 22eV there are two strong and some weaker bands. They result from predissociating Rydberg states. The features with the maximum at 20.23eV and 20.48eV give the most intense contribution to the efficiency curve. These Rydberg states have been observed in absorption spectra (4, 5). Narayana and Price (4) have found ten bands and classified them in three series converging to the limit of 21.72eV. That is the ionization potential for the ion state $c^3\Pi(v'=0)$ (19). They assigned the series as ndπ, npσ, and npπ with $^2\Pi$-symmetry. Sasanuma etal (5) observed twelve bands and classified additional ndσ $^2\Pi$-Rydberg states converging to the same limit. The series are summarized in table 6.

The members of the ndπ series show asymmetric profiles of the Fano-Beutler-type (20) resulting from the interaction of the bound Rydberg states with ionization and dissociation continua. The other series exhibit symmetric profiles.

The corresponding ionization efficiency curves of O^- and N^+ show distinct features related to the 3dπ- and 4pπ/c-

Rydberg states. The 3dπ-state shows an asymmetric profile as in the absorption spectrum. The Rydberg states with higher principal at quantum numbers should be responsible for the appearence of shoulders and small peaks in the O^--yield curve up to 21.5eV (fig 3).

We suggest, that the ion pair state potential energy curve crosses the potential curve of the Rydberg state 3dπ and 4pπ/σ at or near its minimum in the Franck-Condon-region. The ion pair appearing by predissociation of the Rydberg states carries away kinetic energy depending on the position of the Rydberg state above the dissociation limit.

The same Rydberg states give rise to structure in the NO^+- and O^+-efficiency curves observed by Hertz etal (6), as well as in the molecular fluorescence spectra $NO^{+X}(A(v'=0,1) \rightarrow X)$ and in the atomic fluorescence spectra N^X(124,3 nm) observed by Zietz (21). Our data as well as the data of those groups show symmetric profiles of the npπ/σ state as in the absorption spectra. The coupling of the ndπ Rydberg states to the various decay continua seems to be different. The profiles of the ndπ states observed in the different decay channels (table 7) indicate the different ways of coupling to the dissociation and ionization continua.

Above the $c^3\Pi$ state at 21.72eV, ion states with $(\sigma 2s)^{-1}$ and $(\pi 2p)^{-1}$ electronic configurations are expected with $^1\Pi$ and $^1\Sigma^+$- symmetry, respectively. The $^1\Pi$ and $^1\Sigma^+$ ion states have been observed in photoelectron spectra (19). They have been assigned based on a discussion of the vibrational structure and the intensity ratios. A comparison with the isoelectronic molecules CO and N_2 confirmed the interpretation.

In the absorption spectrum there is no evidence for Rydberg states converging to these ion states.

However, there are some features in the O^--efficiency curve, which cannot be assigned in correlation with states

converging to the $c^3\Pi$ NO^+ state. This group of structures consists of bands emerging as shoulders on the low energy side as well as the high energy side of the $4p\pi/\sigma$ Rydberg state. And there is a broad band at 21.9eV.

These new structures are interpreted as a vibrational progression of Rydberg states converging to the $B'^1\Sigma^+$-NO^+ ion state (19). In the photoelectron spectrum, this ion state exhibits thirteen vibrational levels with maximum at 23.31eV. The envelope of this progression shows a fwhm of about 400 meV. Because of the Franck-Condon-principle, the energetic width of the Rydberg states should correspond to the width of the ion state in the case of one-electron-excitation. In fact, the band at 21.9eV shows a width of about 400 meV. The shoulders of the low and high energy side of the $4p\pi/\sigma$ Rydberg state peak are both interpreted as belonging to the same state. These two states are members of a Rydberg series converging to the $B'^1\Sigma^+$-state. The quantum defect of this series amounts to about 0.86. The Rydberg electron should be in a d-orbital, therefore. This result is found for all Rydberg series in NO converging to an ion state with ionized $(\pi 2p)$-electron (22) .

These Rydberg states should predissociate to ion pair states leading to the dissociation limit at 19.56eV or 21.46eV; i.e. O^- in the ground state and N^+ in the ground state or in the first excited ^1D state, respectively, should be formed. A symmetry allowed transition is possible.

The broad bands at 23.1eV and 24.5eV in the O^--efficiency curve have also been observed in electron impact studies (16). Those authors interpreted the structure as due to Franck-Condon-transitions into ion pair states leading to the dissociation limits at 21.46eV and 23.62eV (table 4). The ions should carry away a certain amount of kinetic energy in this case. The combination of the atomics terms rise to molecular states in which dipole allowed transitions are possible.

N^+

Above 21.02eV in addition to ion pair formation, the production of N^+ may occur by dissociative ionization. The lowest dissociation limit is at 21.02eV, where N^+ and a neutral oxygen atom are formed both in the ground state. We interpret the onsets at 21.00eV and 21.34eV observed in the N^+-yield curve (fig 3) as due to preionization of higher members of the Rydberg states converging to the $^3\Pi$-ion state in a repulsive part of an ion state leading to the 21.02eV-dissociation limit (23, 24).

The steep ascent at 21.74eV is due to direct ionization in the $c^3\Pi$-ion state followed by predissociation via ion states leading to the same limit at 21.02eV (23, 24). The same interpretation has been given by Hertz et al (6).

Before the end of the steep onset, we observed at least four small steps (fig 4). Possibly predissociation occurs from the vibrational levels observed in the photoelectron spectrum and assigned as vibrational levels (19) of the $B'^1\Sigma$ ion state. The height of the steps decreases with increasing energy. This resembles the intensity ratio found in the photoelectron spectrum.

All the processes contributing to the N^+-yield above 21.0eV and below 22.92eV form N^+ and neutral oxygen atoms both in the ground state. Above the threshold energy, kinetic energy is carried away by the fragments.

A further ascent at 23.0eV has been observed for the first time. The vibrational levels of the $B'^1\Sigma^+$ ion state occur at 22.72eV. Possible direct ionization is responsible, followed by predissociation to the repulsive part of the $^1\Sigma^+$- and/or $^3\Sigma^+$-states (23, 24), leading to the dissociation limit at 21.0eV. The ascent is quite slow because of the minimum of the potential energy curve at about 1.45 Å (22). The $N^+(^3P) + O(^1D)$- and the $N^+(^1D) + O(^3P)$-dissociation limit at 22.96eV and 22.99eV, respectively, can be reached at this energy as well (table 5).

CO

Results

Ion pair formation processes leading to $O^- + C^+$ and $C^- + O^+$ from carbon monoxide have been studied. The photoionization efficiency curves are shown in fig 5, 6, and 7. The O^--efficiency curve (fig 5) exhibits a steep onset at 20.91eV. There are several steps on the slope. Up to 22.5eV seven intense bands are observed as well as a number of weak features and shoulders. In the energy region 22.5eV to 23.5eV, some weak and broader bands occur. Above 23.5eV, the O^--yield curve increases and three broad structureless bands are observed.

In the corresponding C^+-efficiency curve the same features as observed in the O^--efficiency curve appear up to about 22.4eV. The peak structure is somewhat less distinct because of contributions due to second order radiation from the grating. This contribution smooths the sharp peak structure of the C^+-ion yield curve.

The C^+-efficiency curve above 22.4eV (fig 6) shows a steep increase with several shoulders on the slope. Dissociative ionization of the CO-molecule can occur at this energy. A second ascent is observed at 24.3eV.

The C^--efficiency curve is shown in fig 7. The onset of the yield is determined to lie at 23.45eV. Because the ion pair, C^-/O^+, is formed with very low intensity, the O^+-yield resulting from the ion pair formation is too small for direct observation. The O^+-yield from ion formation processes is also masked by very small contaminations of the CO gas.

The table 8 summarizes the features observed in the O^--efficiency curve and previous results obtained by means of absorption measurements and electron impact studies.

Codling and Potts (7) assigned the absorption bands as Rydberg states converging to two-electron-excited ion states. Locht etal (16) observed the O^--yield in the 20eV to 26eV energy region. Kinetic energy distribution

studies of the C^+ ion have been performed by the same authors (25, 26). They excited the CO-molecule with 22eV electrons and ascribed the observed features to predissociation of $3d\sigma$ or $3p\sigma$ Rydberg states.

In the O^--yield, they observed the threshold at 20.88eV and six further onsets up to 25.4eV. They interpreted these six peaks as due to dissociation to ion pair states.

The agreement with our data is good. There are some features which had not been observed in the absorption spectra. The additional features are accounted for by the proposed Rydberg series, by extrapolation with the known quantum defects.

Discussion

O^-

In the whole investigated energy range, the ion pair fragments O^- and C^+ are formed in the ground state. Excited states of C^+ should appear 5.33eV above the threshold energy of 20.91eV. The structure observed up to 23.5eV is due to Rydberg states predissociating via the repulsive part of the ion pair potential energy curve.

These Rydberg states have been observed in the absorption spectrum (7, 9, 17, 27). The same states have been found in the kinetic energy distribution curves of C^+ (25, 26) and in VUV-fluorescence spectra (28).

Codling and Potts (7) classified the absorption bands using the photoelectron spectrum performed by Potts and Williams (29). Later, a somewhat different assignment of the absorption bands was proposed by Åsbrink etal (30) based on a high resolution photoelectron spectrum.

In the 21eV to 37eV energy region one-electron excited ion states do not exist; structure observed in that energy region by means of UPS-, XPS- or electron energy-loss

measurements is ascribed to two-electron excitation made possible by configuration interaction (31). The assignment and the electron configuration of the two-electron excited ion states of CO observed in the photoelectron spectrum are summarized in table 9. Okuda etal (32) have described the $D^2\Pi$-ion state as having an ionized π2p-electron and a σ2p-electron excited in the π^*2p-orbital, while the $C^2\Sigma^+$-ion state has an ionized σ2p-electron and a π2p-electron excited in the π^*2p orbital. This assignment has been adapted by Potts and Williams (29) and Åsbrink etal (30). Schirmer etal (33) have given a method to calculate weak satellite lines in the photoelectron spectrum in the region of inner valence electron ionization, which does not represent the ionization of an electron out of a particular molecular orbital. They obtained two satellite lines at 22.83eV and 22.93eV, which derive their intensities from the σ^*2s- and σ2p-orbital, respectively. If these lines correspond to the C and D ion states observed in the photoelectron spectra by Åsbrink etal (30), the interpretation differs from Okuda etal (32) and the final assignment of these states remains unsettled. In the following discussion the assignment of Okuda etal (32) is used.

Åsbrink etal (30) arranged the absorption bands in vibrational progressions of the 3p, 4p, and 5p Rydberg states converging to the $D^2\Pi$ state. There were also progressions of the 3s, 4s, 5s, and 3p, and 4p Rydberg states converging to the $C^2\Sigma^+$ ion state. The interpretation of the 3s vibrational progressions converging probably to the $E^2\Sigma^+$ state is still ambiguous. Some bands are unclassified in that assignment.

In this work, relative intensity ratios of the Rydberg states have been measured. The comparison of the Franck-Condon-factors of the photoelectron spectrum and of the Rydberg states supports the assignments performed by Åsbrink etal (30).

C^+

The C^+-efficiency curve (fig 6) shows the same structure as the O^--efficiency curve up to 22.45eV. Above the energy of 22.37eV, C^+ and neutral oxygen atoms, both in the ground state, may be formed. At 22.4eV we observe a steep onset with steps in the slope, followed by a second onset at 24.3eV.

The steps of the first ascent are identified as the vibrational levels of the $D^2\Pi$-ion state: the formation of C^+ in the threshold region above 22.45eV is interpreted as due to predissociation of the $D^2\Pi$ state. Locht (26) observed the same features in the C^+ retarding potential curve. He proposed the $D^2\Pi$-predissociation to occur through a $^2\Delta_r$-state (ref 2 in (25)) leading to the $C^+(^2P^o) + O(^3P)$-dissociation limit.

The onset at 24.3eV is observed by Locht as well (25, 26) and is interpreted here as due to direct dissociation through the $C^2\Sigma^+$-state. The fragments should be $C^+(^2P^o) + O(^1D)$.

C^-

The minimum energy of the ion pair process $C^- + O^+$ is calculated to be 23.45eV, using D(CO) = 11.108eV (34), IP(O) = 13.614eV (35), and EA(C) = 1.272eV (36). The C^--threshold has been observed at 23.34eV in agreement with the calculated value. The C^--efficiency curve shows a broad band with a maximum at 23.8eV. The curve decreases to nearly zero at 24.8eV. The C^-/O^+ ion pair formation occurs in that small energy region only. The $C^-(^4S^o)$ and $O^+(^4S^o)$ atomic states combine to $^{1,3,5,7}\Sigma^+$ molecular states. Probably, at threshold energy, the CO molecule is excited from the $^1\Sigma^+$ ground state directly to the $^1\Sigma^+$-ion pair state, followed by dissociation.

Conclusion

In the photoionization efficiency curves of negative ions, formed in ion pair formation processes from O_2, NO, and CO,

considerable structure is observed. The coupling of super-excited states to ion pair continua is confirmed. For molecular oxygen and nitric oxide new Rydberg series which were undiscernable in absorption spectra, are proposed.

Measurements with high wavelength resolution would give new information on the weak Rydberg series in all the three molecules, and would probably solve the problem of the assignment of two-electron-excited ion states in CO.

Acknowledgement

Financial support of the Bundesministerium für Forschung und Technologie is gratefully acknowledged. The authors are indebted to the Deutsches Elektronen Synchrotron, DESY, for support of the experimental work. We would like to thank R. Zietz for helpful discussions and for assistance in carrying through the measurements.

References

(1) P. M. Dehmer and W. A. Chupka, J. Chem. Phys. 62 (1975) 4525.

(2) K. Codling and R. P. Madden, J. Chem. Phys. 42 (1965) 3935.

(3) W. S. Watson, J. Lang and D. T. Stewart, Phys. Lett. A 44 (1973) 293.

(4) B. Narayana and W. C. Price, J. Phys. B 5 (1972) 1784.

(5) M. Sasanuma, Y. Morioka, E. Ishiguro and M. Nakamura, J. Chem. Phys. 60 (1974) 327.

(6) H. Hertz, E. W. Jochims, H. Schenk and W. Sroka, Chem. Phys. Letters 29 (1974) 572.

(7) K. Codling and A. W. Potts, J. Phys. B7(1974) 163.

(8) L. C. Lee, R. W. Carlson and D. L. Judge, Mol. Phys. 30 (1975) 1941.

(9) M. Sasanuma, E. Ishiguro, Y. Morioka and M. Nakamura, Third Int. Conf. Vacuum Ultraviolet Radiation Physics Tokyo 1974 ed. Y. Nakai (Tokyo: Physical Society of Japan).

(10) P. L. Kronebusch and J. Berkowitz, Intern. J. Mass. Spectry. Ion Phys. 22 (1976) 283.

(11) H. Schenk, H. Oertel and H. Baumgärtel, Ber. Bunsenges. Physik. Chem. 83(1979) 683.

(12) M. Skibowski and W. Steinmann, J. Opt. Soc. Am. 57 (1967) 112.

(13) V. N. Dibeler and J. A. Walker, J. Opt. Soc. Am. 57 (1967) 1007.

(14) F. A. Elder, D. Villarejo and M. G. Inghram, J. Chem. Phys. 43 (1966) 758.

(15) E. Lindholm, Ark Fys. 40 (1969) 117.

(16) R. Locht and J. Momigny, Intern. J. Mass. Spectry. Ion Phys. 7 (1971) 121 and references therein.

(17) L. C. Lee, R. W. Carlson, D. L. Judge and M. Ogawa, J. Chem. Phys. 61 (1974) 3261.

(18) P. M. Hierl and J. L. Franklin, J. Chem. Phys. 47 (1967) 3154.

(19) O. Edqvist, L. Åsbrink and E. Lindholm, Z. Naturforsch. 26a (1971) 1407.

(20) U. Fano, Phys. Rev. 124 (1961) 1866.

(21) R. Zietz, Ph. D. Thesis, University of Kaiserslautern 1978, Int. Bericht DESY F41-78/05, 1978.

(22) O. Edqvist, E. Lindholm, L. E. Selin, H. Sjögren and L. Åsbrink, Ark. Fys. 40 (1970) 439.

(23) D. L. Albritton, A. L. Schmeltekopf and R. N. Zare, J. Chem. Phys. in press.

(24) F. R. Gilmore, J. Quant. Spectrosc. Radiat. Transf. 5 (1965) 369.

(25) R. Locht and J. M. Dürer, Chem. Phys. Letters 34 (1975) 508.

(26) R. Locht, Chem. Phys. 22 (1977) 13.

(27) J. Fock, P. Gürtler and E. E. Koch, to be published.

(28) L. C. Lee, R. W. Carlson, D. L. Judge and M. Ogawa, J. Chem. Phys. 63 (1975) 3987.

(29) A. W. Potts and T. A. Williams, J. Electron Spectry. Relat. Phenom. 3 (1974) 3.

(30) L. Åsbrink, C. Fridh, E. Lindholm and K. Codling, Phys. Scripta 10 (1974) 183.

(31) J. C. Lorquet and C. Cadet, Intern. J. Mass Spectry. Ion Phys. 7 (1971) 245.

(32) M. Okuda and N. Jonathan, J. Electron Spectry. Relat. Phenom. 3 (1974) 19.

(33) J. Schirmer, L. S. Cederbaum, W. Domcke and W. von Niessen, Chem. Phys. 26 (1977) 149.

(34) G. Herzberg, Spectra of Diatomic Molecules (Van Nostrand, Princeton, 1950), p. 521.

(35) C. E. Moore, Ionization Potentials and Ionization Limits Derived from the Analysis of Optical Spectra, NSRDS-NBS 34 (1970).

(36) H. Hotop and W. C. Lineberger, J. Chem. Phys. Ref. Data 4 (1975) 539.

Table 1

Energetic positions (eV) of features observed in the O^--efficiency curve from O_2

	this work		ref 16	ref 2	
	photoionization		electron impact	absorption	
1	20.59±0.03	steep onset	20.6		
2	20.73	peak			
3	20.85	peak		20.862	$3s\sigma_g(0.0)$
4	20.94	peak			
5	21.05	small peak		21.050	$3s\sigma_g(1.0)$
6	21.28	steep onset	21.3		
7	21.70	small peak			
8	21.85	small peak			
9	21.94	onset (?)			
10	22.11	small peak			
11	22.27	small peak			
12	22.46	onset	22.5		
13	22.83	small peak		22.863	$3d\sigma_g(0.0)$
14	22.92	small peak			
15	23.04	small peak		23.050	$3d\sigma_g(1.0)$
16	23.13	shoulder			
17	23.22	peak		23.262	$4s\sigma_g(1.0)$
18	23.34	small peak			
19	23.39	peak			
20	23.79	small peak		23.825	$4d\sigma_g(1.0)$
			23.55		
			23.9		
			25.2		

Table 2

New Rydberg states converging to the $c^4\Sigma_u^-$-ion state.
The numbers of the peaks of table 1 are given in brackets. Energetic values in eV.

vibrational transition	n = 3	n = 4	quantum defect δ
(0,0)	21.70 (7)	23.20 (17)	
(1,0)	21.85 (8)	23.39 (19)	0.83
(0,0)	22.22 (10)	23.34 (18)	
(1,0)	22.27 (11)	23.53 (-)	0.65

Table 3

Energetic positions (eV) of features observed in the O^--efficiency curve from NO

	this work		ref 16	ref 18	ref 4	
	photoionization		electron impact	electron impact	absorption	
1	19.56±0.03	steep onset	19.6+0.2	19.3±0.3		
2	20.10	shoulder				
3	20.23	peak			20.242	3dπ
4	20.33	small peak				
5	20.48	peak			20.486	4pπ
6	20.63	shoulder				
7	20.69	shoulder				
8	20.84	small peak			20.78[a]	4dσ
9	20.92	small peak			20.897	4dπ
10	21.00	small peak			20.993	5pπ
11	21.13	small peak				
12	21.21	small peak			21.190	5dπ
13	21.26	small peak			21.245	6pπ
14	21.31	small peak				
15	21.37	small peak			21.354	6dπ
16	21.45	shoulder			21.450	7dπ
17	21.49	steep onset	21.4[b]			
18	21.9±0.1[c]	broad peak				
19	23.1±0.1[c]	broad peak	23.1[d]			
20	24.5±0.1[c]	broad peak	24.0[b]			

a) ref 5
b) threshold
c) maximum of the broad peak
d) maximum of the peak

Table 4

Threshold energies (eV) for ion pair formation from NO

1	19.565	$N^+(^3P) + O^-(^2P^o)$
2	21.464	$N^+(^1D) + O^-(^2P^o)$
3	23.618	$N^+(^1S) + O^-(^2P^o)$

Table 5

Energetic positions (eV) of features observed above 21eV in the N^+-efficiency curve, and threshold energies of dissociative ionization processes

			threshold energy	fragments
1	21.00±0.05	onset	21.02	$N^+(^3P) + O(^3P)$
2	21.34+0.05	onset		
3	21.74±0.03	steep onset		
4	22.9 ±0.1	onset	22.92	$N^+(^1D) + O(^3P)$
			22.98	$N^+(^3P) + O(^1D)$

Table 6

Rydberg series converging to the $c^3\Pi$ NO^+ state (in the symmetry assignment we follow Narayama and Price (4))

assignment		quantum defect	intensity
nsπ	$^2\Pi$	-0.03	strong
npσ	$^2\Pi$	0.72	medium
npπ	$^2\Sigma$	0.78	medium
ndσ	$^2\Pi$	0.19	weak

Table 7
Profiles of the nlπ-Rydberg states observed in different decay channels

	decay channel	profile	ref
1	O^-	asymmetric	this work
2	NO^+	asymmetric	(6)
3	O^+	symmetric	(6)
4	$NO^+(X(v'=0) \rightarrow X)$	asymmetric	(21)
5	$NO^+(X(v' \neq 0) \rightarrow X)$	symmetric	(21)
6	N^X (124.3nm) (+O)	symmetric	(21)
	absorption spectrum	asymmetric	(4)

Table 8

Energetic positions (eV) features observed in the O^--efficiency curve from CO

	this work		ref 16	ref 7
	photoionization		electron impact	absorption
1	20.94±0.02	shoulder	20.88±0.02	20.936
2	21.07	shoulder		21.068
3	21.13±0.01	peak		21.126
4	21.27	peak		21.241
5	21.31	shoulder		21.313
6	21.42	small peak		21.416
7	21.52	peak		21.475
8	21.61	peak		21.604
9	21.65	shoulder		21.653
10	21.74	small peak		21.743
11	21.82	peak		21.823
12	21.86	shoulder		
13	21.93	shoulder		
14	22.04	small peak		22.049
15	22.11	shoulder		22.098
16	22.13	peak		22.164
17	22.28	peak		22.254
18	22.40	shoulder		
19	22.42	small peak		22.415
20	22.50	small peak		22.495
21	22.63	small peak		22.580
22	22.68	small peak		
23	22.80	small peak		
24	22.93	small peak		22.915
25	23.22	small peak		
26	23.38	small peak		
27	23.72±0.05	onset	22.65 [a]	
28	24.2 ±0.08	onset	24.1 [a]	
29	24.9 ±0.08	onset	24.6 [a]	
			22.8 [a]	
			23.1 [a]	
			25.3 [a]	

a) position of the maximum of the peak

Table 9

The ionization potentials and the regions of vibrational progressions of two-electron-excited ion states in CO (eV)

The ground state of the neutral CO molecule may be written as KK $(\sigma 2s)^2 (\sigma^* 2s)^2 (\pi 2p)^4 (\sigma 2p)^2\ ^1\Sigma^+$. Configurations of the ion states correspond to the number of the electrons in the orbitals $(\sigma 2s)(\sigma^* 2s)(\pi 2p)(\sigma 2p)(\pi^* 2p)(\sigma^* 2p)$, in that order.

vertical ionization potential	region of the vibrational progressions	calculated IP_{vert}	electron configuration and symmetry of the ion state	
ref 30	ref 30	ref 32		
22.73	22.04 - 23.23	20.33	222210	$D\ ^2\Pi$
23.38	23.04 - 23.99	22.19	223110	$C\ ^2\Sigma^+$
25.48	24.77 - 26.53	26.11	223110	$(E)\ ^2\Sigma^+$
28.09	27.7 - 28.43	29.62	213210	$(F)\ ^2\Sigma^+$
CO ground state			224200	$^1\Sigma^+$

Figure Captions

Figure 1 O^+- and O^--efficiency curves from O_2. The O^+-yield curve is reduced here by a factor of 40. The curves cross at 18.5eV (67 nm).

Figure 2 O^--efficiency curve from O_2 in the 20eV to 27eV energy region.

Figure 3 N^+- and O^--efficiency curves from NO. The N^+-yield curve is reduced by a factor of 7. The curves cross at 19.6eV and again between 21.3eV and 21.8eV.

Figure 4 N^+-efficiency curve from NO in the 18eV to 25eV energy region.

Figure 5 C^+- and O^--efficiency curves from CO. The C^+-yield curve is reduced by a factor of 6. The curves cross at 21eV and 22.5eV.

Figure 6 C^+-efficiency curve from CO in the 20eV to 26eV energy region.

Figure 7 C^--efficiency curve from CO in the 23eV to 25eV energy region.

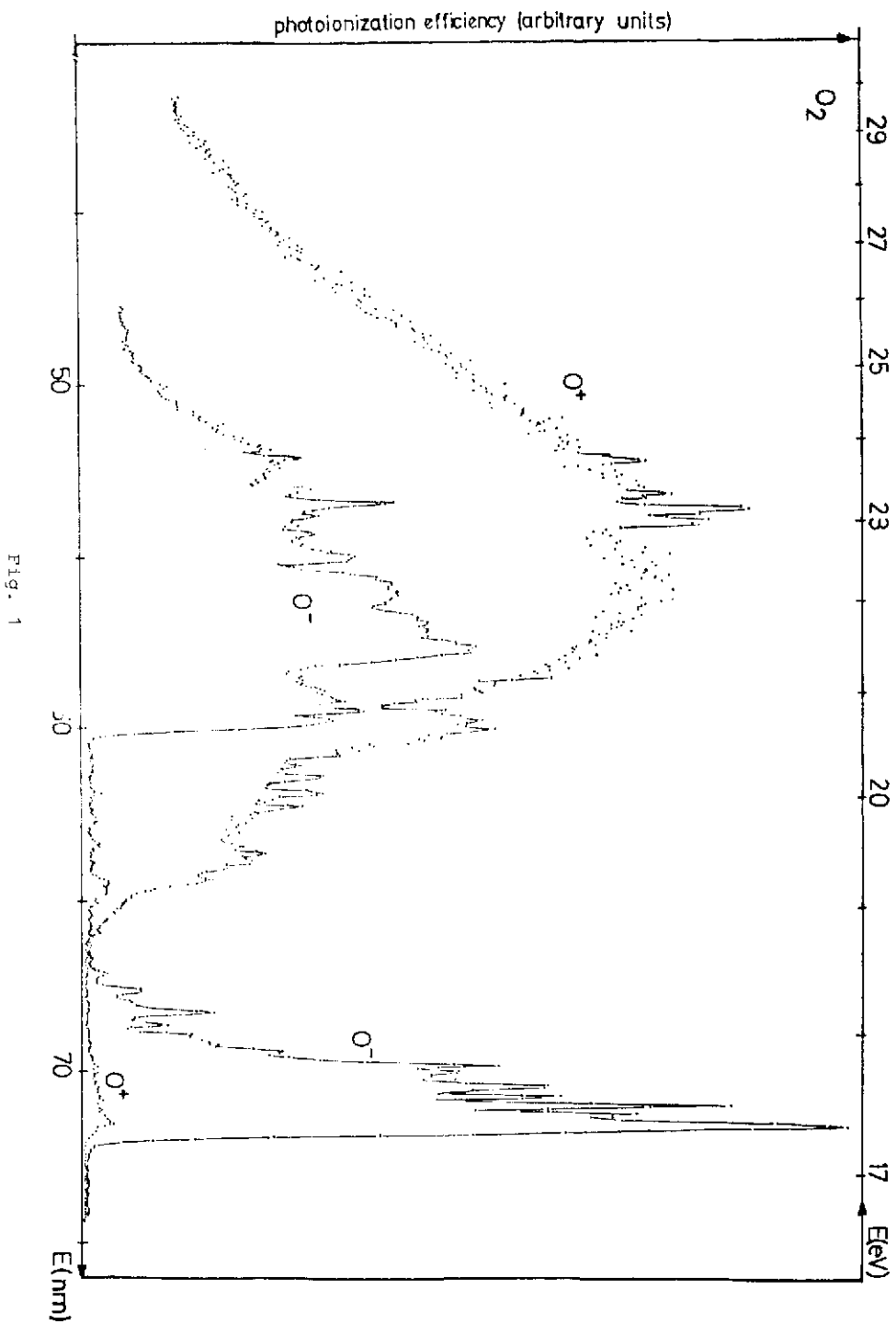

Fig. 1

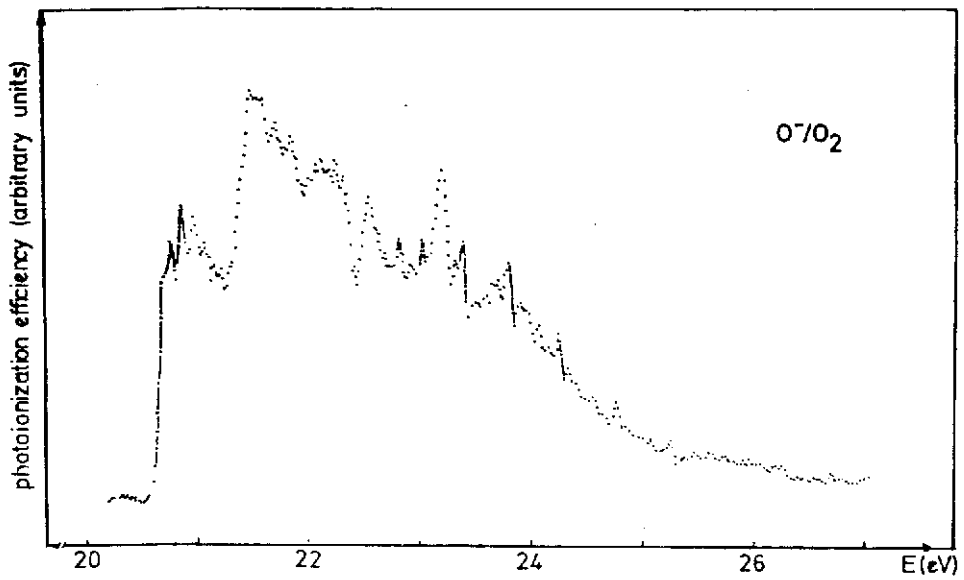
photoionization efficiency (arbitrary units)
O^-/O_2
20
22
24
26
E(eV)

Fig. 2

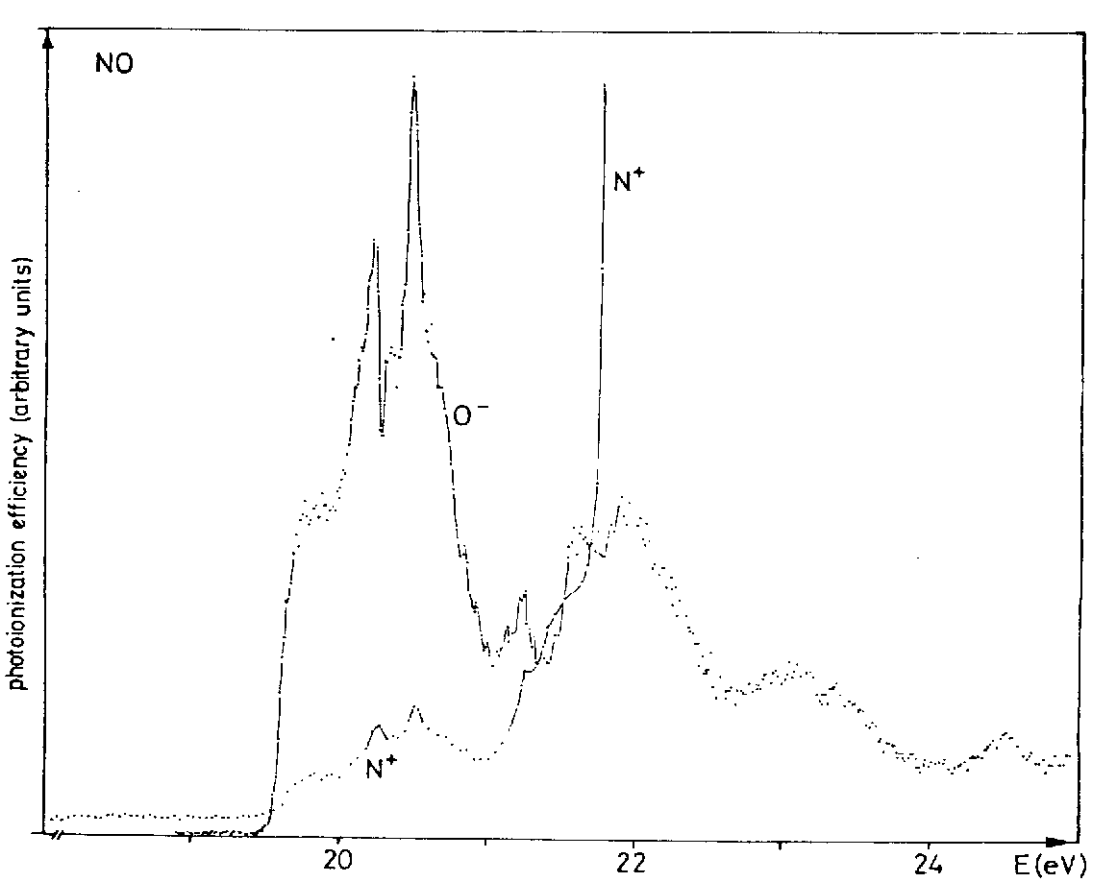
NO
N^+
O^-
N^+
photoionization efficiency (arbitrary units)
20
22
24
E(eV)

Fig. 3

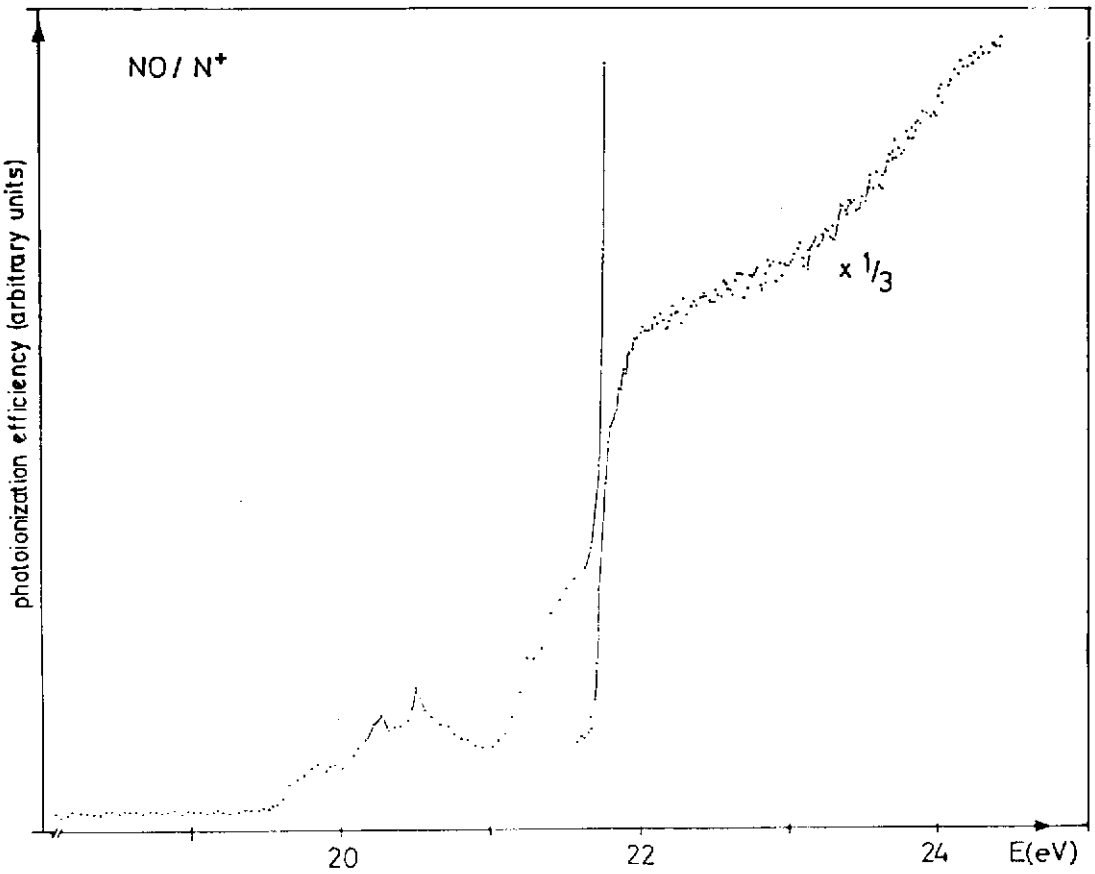
NO / N+
photoionization efficiency (arbitrary units)
x 1/3
20
22
24
E(eV)

Fig. 4

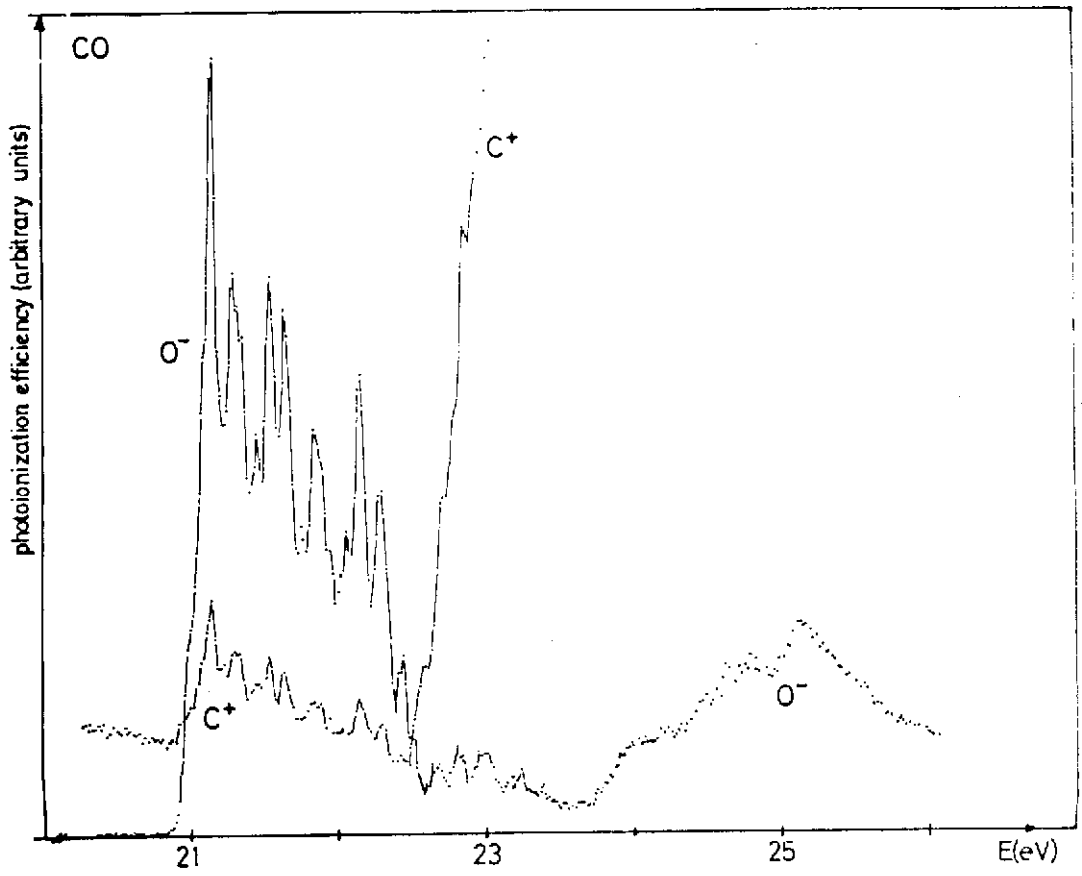
CO
photoionization efficiency (arbitrary units)
C+
O-
C+
O-
21
23
25
E(eV)

Fig. 5

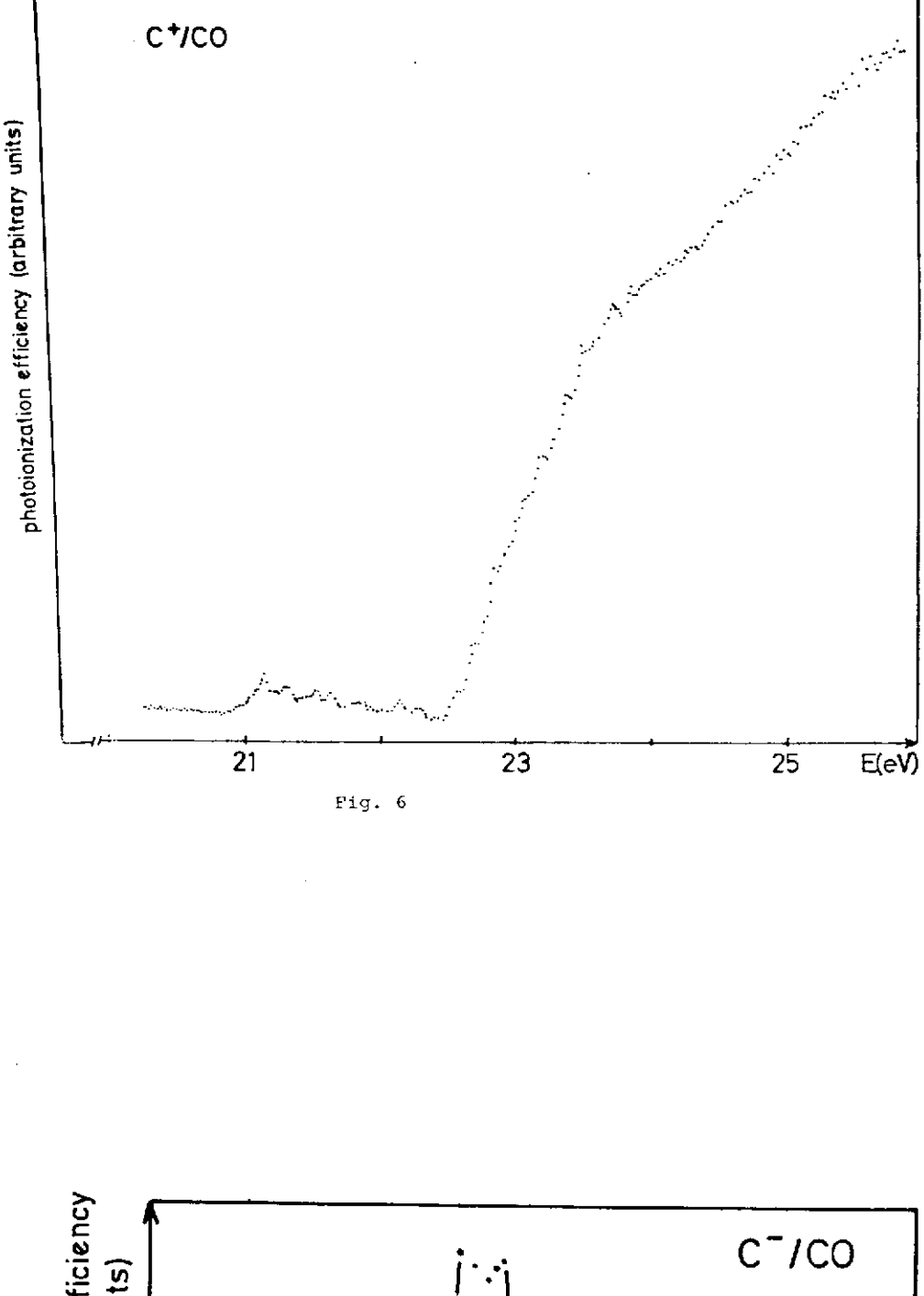
C+/CO
photoionization efficiency (arbitrary units)
21
23
25
E(eV)

Fig. 6

C⁻/CO
photoionization efficiency
(arbitrary units)
23
25
E(eV)

Fig. 7